Relativistic Auger and x-ray emission rates of the $1s\,2l^n(2l')^m$ configurations of Be-like ions

Mau Hsiung Chen
Lawrence Livermore National Laboratory, University of California, Livermore, California 94550
(Received 5 November 1984)

Properties of the $1s\,2l^n(2l')^m$ $(n+m=3)$ states of Be-like ions are calculated relativistically for $6\leq Z\leq 26$ using multiconfiguration Dirac-Fock method. Generalized Breit interaction and quantum-electrodynamic corrections are taken into account in the calculations of energies. Transition rates are computed in intermediate coupling with configuration interaction. The generalized Breit interaction is included both in the evaluation of mixing coefficients and relativistic Auger matrix elements. The contributions of the radiationless transitions to the decay of the metastable quintet states are found to be very significant. The effects of relativity and configuration interaction on the transition rates are discussed.

I. INTRODUCTION

The properties of multiply ionized atoms are very important in connection with astrophysics and with the physics of atomic collisions and fusion plasmas. The Auger and x-ray spectra of the Li-like $1s\,2l\,2l'$ configurations have been thoroughly studied.[1–10] The effect of relativity has been found to have a pronounced influence on the transition rates of some of the multiplet states, especially for the metastable states.[5,9,10]

Recently, the radiative transitions

$$1s\,2s\,2p^2\,{}^5P_{1,2,3}-1s\,2p^3\,{}^5S_2$$

have been observed.[11–14] The measured wavelengths, fine structure, and decay times were compared with the results from multiconfiguration Dirac-Fock (MCDF) calculations.[11–14] However, in the existing calculations of the lifetime of the $1s\,2p^3\,{}^5S_2$ state, only the lifetime from radiative decay was taken into account. The contributions from Auger decay were completely ignored. Although the $1s\,2p^3\,{}^5S_2$ is Auger forbidden in the nonrelativistic limit, it can decay by spin-orbit mixing with singlet and triplet states or through the Breit interaction in the relativistic calculations. Several nonrelativistic calculations[15,16] have been performed for $1s\,2l^n(2l')^m(n+m=3)$ configurations of Be-like ions to predict x-ray and Auger transition energies and transition rates. There exist no relativistic calculations of Auger transition rates for $1s\,2l^n2l'^m$ configurations of Be-like ions.

In this paper we report on the relativistic calculations of multiplet Auger and x-ray energies and transition rates. The calculations were performed in the intermediate-coupling with configuration interaction using the MCDF method[17] for the $1s\,2p^3$, $1s\,2s\,2p^2$, and $1s\,2s^2\,2p$ configurations of Be-like ions for eight elements with atomic numbers $6\leq Z\leq 26$.

II. THEORY

A. Relativistic Auger transition rates

The radiationless transition probability is calculated from perturbation theory.[18,19] The transition rate in frozen-orbital approximation is given by

$$T=\frac{2\pi}{\hbar}\left|\left\langle\psi_f\left|\sum_{\alpha<\beta}V_{\alpha\beta}\right|\psi_i\right\rangle\right|^2\rho(\epsilon)\ . \tag{1}$$

Here, ψ_i and ψ_f are the antisymmetrized many-electron wave functions of the initial and final states of the ion, respectively; $\rho(\epsilon)$ is the energy density of final states; and $V_{\alpha\beta}$ is the two-electron interaction operator.

In the present work, the two-electron operator $V_{\alpha\beta}$ is taken to be the sum of Coulomb and generalized Breit operator:[20,21]

$$V_{12}=\frac{1}{r_{12}}-\boldsymbol{\alpha}_1\cdot\boldsymbol{\alpha}_2\frac{\cos(\omega r_{12})}{r_{12}} +(\boldsymbol{\alpha}_1\cdot\boldsymbol{\nabla}_1)(\boldsymbol{\alpha}_2\cdot\boldsymbol{\nabla}_2)\frac{\cos(\omega r_{12})-1}{\omega^2 r_{12}}\ , \tag{2}$$

where $\mathbf{r}_1$ and $\mathbf{r}_2$ are particle position vectors; $\mathbf{r}_{12}=\mathbf{r}_1-\mathbf{r}_2$; and $\boldsymbol{\nabla}_1$ and $\boldsymbol{\nabla}_2$ are gradient operators corresponding to $\mathbf{r}_1$ and $\mathbf{r}_2$, respectively. The $\boldsymbol{\alpha}_i$ are Dirac matrices, and ω is the wave number of the exchanged virtual photon. In Eq. (2) and hereafter, atomic units are used unless specified otherwise.

In the restricted Hartree-Fock scheme, the N-electron wave function is constructed from central-field Dirac orbitals given by

$$\psi_{nkm}(r)=\frac{1}{r}\begin{bmatrix}P_{nk}(r)\Omega_{km}\\ iQ_{nk}(r)\Omega_{-km}\end{bmatrix}\ , \tag{3}$$

where

$$\Omega_{km}=\sum_{\mu}C(l\,\tfrac{1}{2}\,j;m-\mu,\mu)Y_{l,m-\mu}(\theta,\phi)\chi_{1/2,\mu}\ , \tag{4}$$

with

$$k=(l-j)(2j+1)\ . \tag{5}$$

In the MCDF model,[17] the configuration state functions (CSF's) denoted by $\phi(\Gamma JM)$ are formed by taking linear combinations of Slater determinants of the orbitals; an

TABLE I. Calculated K x-ray energies (in eV) for the $1s\,2l^n2l'^m$ $(n+m=3)$ configurations of Be-like ions.

Transition	$_6C^{+2}$	$_7N^{+3}$	$_8O^{+4}$	$_9F^{+5}$	$_{10}Ne^{+6}$	$_{12}Mg^{+8}$
$1s^22p^2$-$1s\,2p^3$						
^3P-^5S	285.20	402.75	540.79	699.31	878.34	1298.09
^1D-^5S	282.81	399.77	537.22	695.17	873.63	1292.23
^3P-^3S	290.33	409.63	549.44	709.74	890.58	1313.93
^3P-^3P	294.00	413.72	553.92	714.59	895.80	1319.89
^1S-^1P	288.63	407.45	546.75	706.56	886.89	1309.24
^1D-^1P	294.17	414.17	554.67	715.67	897.19	1321.89
^3P-^3D	290.05	408.91	548.25	708.08	888.44	1310.80
^1D-^1D	290.21	409.36	549.00	709.16	889.82	1312.80
$^3P_2$-$^1D_2$	292.61	412.34	552.56	713.27	894.50	1318.56
$^1D_2$-$^3P_2$	291.60	410.73	550.34	710.45	891.07	1314.03
$1s^22s\,2p$-$1s\,2s\,2p^2$						
^3P-^5P	284.03	401.67	539.76	698.33	877.40	1297.16
^3P-$(^3S)^3P$	290.54	410.13	550.20	710.76	891.84	1315.62
^3P-^3D	291.75	411.25	551.19	711.61	892.53	1316.04
^3P-^3S	295.31	415.69	556.50	717.80	899.60	1324.85
^1P-^1D	288.41	407.44	546.95	706.96	887.48	1310.20
^3P-$(^1S)^3P$	298.17	418.89	560.02	721.64	903.75	1329.63
^1P-^1S	292.01	411.92	552.31	713.20	894.60	1319.11
^1P-^1P	292.12	411.92	552.19	712.94	894.20	1318.37
$^3P_2$-$^1D_2$	296.34	417.03	558.17	719.79	901.92	1327.79
$^1P_1$-$(^1S)^3P_2$	290.24	409.29	548.80	708.79	889.30	1312.01
$1s^22s^2$-$1s\,2s^22p$						
$^1S_0$-$^3P_1$	289.74	408.95	548.59	708.69	889.27	1312.03
$^1S_0$-$^1P_1$	292.49	412.59	553.15	714.17	895.70	1320.39

atomic state function (ASF) for a state i with total angular momentum JM is then constructed from CSF:

$$\psi_i(JM)=\sum_{\lambda=1}^{n} C_{i\lambda}\phi(\Gamma_\lambda JM)\ , \tag{6}$$

where n is the number of CSF's included in the expansion and $C_{i\lambda}$ are the mixing coefficients for state i.

The Auger transition rate from initial ionic state i to the final ionic state f with continuum orbital j_c is given by

TABLE II. Calculated K x-ray energies (in eV) for the $1s\,2l^n2l'^m$ $(n+m=3)$ configuration of $_{48}Ar^{+14}$ and $_{26}Fe^{+22}$ ions.

Transition	$_{18}Ar^{+14}$	$_{26}Fe^{+22}$	Transition	$_{18}Ar^{+14}$	$_{26}Fe^{+22}$	Transition	$_{18}Ar^{+14}$	$_{26}Fe^{+22}$
$1s^22p^2$-$1s\,2p^3$			$1s^22p^2$-$1s\,2p^3$			$1s^22s\,2p$-$1s\,2s\,2p^2$		
$^3P_1$-$^5S_2$	3054.49	6572.10	$^3P_2$-$^1D_2$	3085.68	6615.39	$^3P_0$-$^3S_1$	3098.51	6641.04
$^3P_2$-$^5S_2$	3052.86	6566.30	$^1D_2$-$^3P_2$	3080.15	6613.30	$^3P_1$-$^3S_1$	3097.64	6637.20
$^1D_2$-$^5S_2$	3044.02	6549.28	$1s^22s\,2p$-$1s\,2s\,2p^2$			$^3P_2$-$^3S_1$	3095.59	6625.84
$^3P_0$-$^3S_1$	3082.02	6620.80	$^3P_0$-$^5P_1$	3053.02	6567.91	$^1P_1$-$^1D_2$	3074.23	6599.22
$^3P_1$-$^3S_1$	3080.81	6612.23	$^3P_1$-$^5P_1$	3052.14	6564.07	$^3P_1$-$(^1S)^3P_0$	3102.58	6639.35
$^3P_2$-$^3S_1$	3079.18	6606.43	$^3P_2$-$^5P_1$	3050.09	6552.72	$^3P_0$-$(^1S)^3P_1$	3104.98	6655.56
$^3P_1$-$^3P_0$	3089.40	6626.42	$^3P_1$-$^5P_2$	3053.44	6571.60	$^3P_1$-$(^1S)^3P_1$	3104.10	6651.72
$^3P_0$-$^3P_1$	3090.62	6636.88	$^3P_2$-$^5P_2$	3051.40	6560.24	$^3P_2$-$(^1S)^3P_1$	3102.06	6640.37
$^3P_1$-$^3P_1$	3089.41	6628.31	$^3P_2$-$^5P_3$	3052.79	6566.70	$^3P_1$-$(^1S)^3P_2$	3105.88	6658.98
$^3P_2$-$^3P_1$	3087.77	6622.51	$^3P_1$-$(^3S)^3P_0$	3082.38	6609.53	$^3P_2$-$(^1S)^3P_2$	3103.83	6647.62
$^3P_1$-$^3P_2$	3090.62	6636.12	$^3P_0$-$(^3S)^3P_1$	3085.33	6617.25	$^1P_1$-$^1S_0$	3089.36	6628.63
$^3P_2$-$^3P_2$	3088.99	6630.32	$^3P_1$-$(^3S)^3P_1$	3084.46	6613.42	$^1P_1$-$^1P_1$	3087.05	6621.24
$^1S_0$-$^1P_1$	3072.54	6599.90	$^3P_2$-$(^3S)^3P_1$	3082.41	6602.06	$^3P_2$-$^1D_2$	3100.76	6635.81
$^1D_2$-$^1P_1$	3092.22	6628.11	$^3P_1$-$(^3S)^3P_2$	3085.79	6627.24	$^1P_1$-$(^1S)^3P_2$	3077.29	6611.03
$^3P_0$-$^3D_1$	3076.36	6609.32	$^3P_2$-$(^3S)^3P_2$	3083.74	6615.89	$1s^22s^2$-$1s\,2s^22p$		
$^3P_1$-$^3D_1$	3075.15	6600.74	$^3P_0$-$^3D_1$	3083.76	6624.47	$^1S_0$-$^3P_1$	3075.59	6596.55
$^3P_2$-$^3D_1$	3073.51	6594.94	$^3P_1$-$^3D_1$	3082.88	6620.63	$^1S_0$-$^1P_1$	3090.66	6627.39
$^3P_1$-$^3D_2$	3075.16	6602.41	$^3P_2$-$^3D_1$	3080.84	6609.27			
$^3P_2$-$^3D_2$	3073.52	6596.60	$^3P_1$-$^3D_2$	3083.24	6615.76			
$^3P_2$-$^3D_3$	3073.25	6598.60	$^3P_2$-$^3D_2$	3081.20	6604.40			
$^1D_2$-$^1D_2$	3076.84	6598.37	$^3P_2$-$^3D_3$	3081.52	6608.53			

TABLE III. Mean transition wavelengths (nm) for $1s\,2s\,2p^2\,{}^5P-1s\,2p^3\,{}^5S$ transitions.

Ion	Experiment	OL[a]	30 EAL[a]	40 EAL[b]
$_6C^{+2}$	101.606±0.005[c]	98.9	100.37	100.81
$_7N^{+3}$	82.565±0.005[c]	80.7	81.64	82.00
$_8O^{+4}$	69.475±0.010[c]	68.2	68.81	69.09
$_9F^{+5}$	59.967±0.010[d]	58.9	59.43	59.66
$_{10}Ne^{+6}$	52.665±0.010[e]	52.0	52.26	52.45
$_{12}Mg^{+8}$				42.09
$_{18}Ar^{+14}$				25.64
$_{26}Fe^{+22}$				15.50

[a]From Ref. 30.
[b]Present work.
[c]From Ref. 12.
[d]From Ref. 32.
[e]From Ref. 30.

$$T_{fi}=\left|\sum_{\lambda}\sum_{\lambda'}C_{i\lambda}C_{f\lambda'}A_{\lambda\lambda'}\right|^2, \tag{7}$$

where

$$A_{\lambda\lambda'}=\left\langle\phi(\Gamma_{\lambda'}J'M')\epsilon j_c;JM\left|\sum_{\alpha<\beta}V_{\alpha\beta}\right|\phi(\Gamma_\lambda JM)\right\rangle . \tag{8}$$

Here, the continuum wave function ϵj_c is normalized to represent one ejected electron per unit time.

The Auger matrix elements $A_{\lambda\lambda'}$ between two CSF's can be separated by tensor algebra into angular parts multiplied by radial integrals by using Fano's procedure.[22] A general computer code[17,23] to evaluate these angular factors is also available.

B. Relativistic radiative transitions

The spontaneous transition probability for a discrete transition $i\rightarrow f$ in multipole expansion is given by perturbation theory to be[24–26]

$$W_{fi}=\frac{1}{2J_i+1}\sum_{M_i,M_f}2\pi\left|\sum_{L,M}\langle f\,|\,T_{LM}\,|\,i\rangle\right|^2 . \tag{9}$$

Since there is no interference between multipoles, Eq. (9) simplifies to

$$W_{fi}=\frac{1}{2J_i+1}\sum_{L}\frac{2\pi}{2L+1}\,|\,\langle f||T_L||i\rangle\,|^2 . \tag{10}$$

In the MCDF model,[17] the reduced matrix element can be expressed in terms of CSF basis:

TABLE IV. Calculated K Auger energies (in eV) for the $1s\,2l^n2l^m$ $(n+m=3)$ configurations of Be-like ions.

Transition	$_6C^{+2}$	$_7N^{+3}$	$_8O^{+4}$	$_9F^{+5}$	$_{10}Ne^{+6}$	$_{12}Mg^{+8}$
$1s\,2p^3$-$1s^22p$						
^5S-^2P	249.21	339.88	444.18	562.28	693.81	998.32
^3D-^2P	254.06	346.04	451.66	570.93	703.90	1011.03
^3S-^2P	254.35	346.75	452.82	572.58	706.03	1014.12
^1D-^2P	256.62	349.46	455.96	576.14	710.00	1018.89
^3P-^2P	258.01	350.85	457.31	577.43	711.25	1020.10
^1P-^2P	260.58	354.28	461.63	582.65	717.37	1027.98
$1s\,2s\,2p^2$-$1s^22p$						
^5P-^2P	236.92	324.76	426.22	541.35	670.13	968.86
$(^3S)^3P$-^2P	243.42	333.21	436.66	553.78	684.57	987.22
^3D-^2P	244.63	334.33	437.66	554.64	685.28	987.68
^3S-^2P	248.19	338.77	442.97	560.82	692.34	996.45
^1D-^2P	249.23	340.12	444.65	562.84	694.71	999.54
$(^1S)^3P$-^2P	251.06	341.97	446.49	564.65	696.48	1001.23
^1S-^2P	252.82	344.60	450.01	569.08	701.83	1008.44
^1P-^2P	252.94	344.60	449.89	568.82	701.42	1007.70
$1s\,2s\,2p^2$-$1s^22s$						
^5P-^2S	245.00	334.84	438.33	555.47	686.31	989.16
$(^3S)^3P$-^2S	251.50	343.29	448.76	567.89	700.71	1007.51
^3D-^2S	252.71	344.41	449.74	568.74	701.42	1007.97
^3S-^2S	256.27	348.85	455.06	574.92	708.47	1016.74
^1D-^2S	257.31	350.21	456.74	576.95	710.84	1019.83
$(^1S)^3P$-^2S	259.14	352.05	458.58	578.76	712.62	1021.52
^1S-^2S	260.90	354.69	462.10	583.19	717.96	1028.73
^1P-^2S	261.02	354.69	461.98	582.93	717.56	1027.99
$1s\,2s^22p$-$1s^22p$						
^3P-^2P	235.81	323.36	424.54	539.38	667.83	965.76
^1P-^2P	238.54	326.99	429.07	544.80	674.17	973.93
$1s\,2s^22p$-$1s^22s$						
^3P-^2S	243.89	333.45	436.63	553.47	683.97	986.06
^1P-^2S	246.63	337.08	441.16	558.90	690.31	994.22

TABLE V. Calculated K Auger energies (in eV) for the $1s2l^n2l'^m$ ($n+m=3$) configurations of $_{18}Ar^{+14}$ and $_{26}Fe^{+22}$ ions.

Transition	$_{18}Ar^{+14}$	$_{26}Fe^{+22}$	Transition	$_{18}Ar^{+14}$	$_{26}Fe^{+22}$	Transition	$_{18}Ar^{+14}$	$_{26}Fe^{+22}$	Transition	$_{18}Ar^{+14}$	$_{26}Fe^{+22}$	Transition	$_{18}Ar^{+14}$	$_{26}Fe^{+22}$
$1s2p^3-1s^22p$			$1s2p^3-1s^22p$			$1s2s2p^2-1s^22s$			$1s2s2p^2-1s^22p$			$1s2s^22p-1s^22s$		
$^5S_2-{}^2P_{1/2}$	2245.94	4702.60	$^1P_1-{}^2P_{1/2}$	2294.15	4781.43	$^1P_1-{}^2S$	2291.40	4767.48	$^3D_3-{}^2P_{1/2}$	2227.32	4669.39	$^3P_0-{}^2S$	2221.17	4645.48
$^5S_2-{}^2P_{3/2}$	2242.78	4686.66	$^1P_1-{}^2P_{3/2}$	2290.99	4765.49	$1s2s2p^2-1s^22p$						$^3P_1-{}^2S$	2221.74	4647.38
$^3D_1-{}^2P_{1/2}$	2266.60	4731.24	$1s2s2p^2-1s^22s$			$^5P_1-{}^2P_{1/2}$	2195.89	4613.58	$^3D_3-{}^2P_{3/2}$	2224.16	4653.45	$^3P_2-{}^2S$	2224.13	4660.62
$^3D_1-{}^2P_{3/2}$	2263.44	4715.30	$^5P_1-{}^2S$	2227.91	4662.37	$^5P_1-{}^2P_{3/2}$	2192.73	4597.64	$^3S_1-{}^2P_{1/2}$	2241.39	4686.70	$^1P_1-{}^2S$	2236.81	4678.21
$^3D_2-{}^2P_{1/2}$	2266.61	4732.90	$^5P_2-{}^2S$	2229.21	4669.89	$^5P_2-{}^2P_{1/2}$	2197.20	4621.10	$^3S_1-{}^2P_{3/2}$	2238.23	4670.76	$1s2s^22p-1s^22p$		
$^3D_2-{}^2P_{3/2}$	2263.45	4716.96	$^5P_3-{}^2S$	2230.61	4676.35	$^5P_2-{}^2P_{3/2}$	2194.04	4605.16	$^1D_2-{}^2P_{1/2}$	2246.56	4696.67	$^3P_0-{}^2P_{1/2}$	2189.15	4596.69
$^3D_3-{}^2P_{1/2}$	2266.34	4734.90	$(^3S)^3P_0-{}^2S$	2258.15	4707.82	$^5P_3-{}^2P_{1/2}$	2198.59	4627.56	$^1D_2-{}^2P_{3/2}$	2243.40	4680.73	$^3P_0-{}^2P_{3/2}$	2185.15	4580.75
$^3D_3-{}^2P_{3/2}$	2263.18	4718.96	$(^3S)^3P_1-{}^2S$	2260.23	4711.71	$^5P_3-{}^2P_{3/2}$	2195.43	4611.62	$(^1S)^3P_0-{}^2P_{1/2}$	2246.34	4688.86	$^3P_1-{}^2P_{1/2}$	2189.72	4598.59
$^3S_1-{}^2P_{1/2}$	2272.26	4742.73	$(^3S)^3P_2-{}^2S$	2261.56	4725.54	$(^3S)^3P_0-{}^2P_{1/2}$	2226.14	4659.03	$(^1S)^3P_0-{}^2P_{3/2}$	2243.18	4672.92	$^3P_1-{}^2P_{3/2}$	2186.56	4582.65
$^3S_1-{}^2P_{3/2}$	2269.10	4726.79	$^3D_1-{}^2S$	2258.66	4718.92	$(^3S)^3P_0-{}^2P_{3/2}$	2222.98	4643.09	$(^1S)^3P_1-{}^2P_{1/2}$	2247.86	4701.23	$^3P_2-{}^2P_{1/2}$	2192.12	4611.83
$^1D_2-{}^2P_{1/2}$	2278.77	4751.69	$^3D_2-{}^2S$	2259.02	4714.05	$(^3S)^3P_1-{}^2P_{1/2}$	2228.21	4662.92	$(^1S)^3P_1-{}^2P_{3/2}$	2244.70	4685.29	$^3P_2-{}^2P_{3/2}$	2188.96	4595.89
$^1D_2-{}^2P_{3/2}$	2275.61	4735.75	$^3D_3-{}^2S$	2259.33	4718.18	$(^3S)^3P_1-{}^2P_{3/2}$	2225.05	4646.98	$(^1S)^3P_2-{}^2P_{1/2}$	2249.63	4708.49	$^1P_1-{}^2P_{1/2}$	2204.79	4629.42
$^3P_0-{}^2P_{1/2}$	2280.85	4756.92	$^3S_1-{}^2S$	2273.41	4735.49	$(^3S)^3P_2-{}^2P_{1/2}$	2229.54	4676.75	$(^1S)^3P_2-{}^2P_{3/2}$	2246.47	4692.55	$^1P_1-{}^2P_{3/2}$	2201.63	4613.48
$^3P_0-{}^2P_{3/2}$	2277.69	4740.98	$^1D_2-{}^2S$	2278.58	4745.46	$(^3S)^3P_2-{}^2P_{3/2}$	2226.38	4660.81	$^1S_0-{}^2P_{1/2}$	2261.70	4726.08			
$^3P_1-{}^2P_{1/2}$	2280.86	4758.81	$(^1S)^3P_0-{}^2S$	2278.36	4737.65	$^3D_1-{}^2P_{1/2}$	2226.64	4670.13	$^1S_0-{}^2P_{3/2}$	2258.54	4710.15			
$^3P_1-{}^2P_{3/2}$	2277.70	4742.87	$(^1S)^3P_1-{}^2S$	2279.88	4750.02	$^3D_1-{}^2P_{3/2}$	2223.48	4654.19	$^1P_1-{}^2P_{1/2}$	2259.39	4718.70			
$^3P_2-{}^2P_{1/2}$	2282.07	4766.62	$(^1S)^3P_2-{}^2S$	2281.65	4757.27	$^3D_2-{}^2P_{1/2}$	2227.00	4665.26	$^1P_1-{}^2P_{3/2}$	2256.23	4702.76			
$^3P_2-{}^2P_{3/2}$	2278.91	4750.68	$^1S_0-{}^2S$	2293.71	4774.87	$^3D_2-{}^2P_{3/2}$	2223.84	4649.32						

TABLE VI. Theoretical Auger x-ray transition rates (in multiple of 10^{12} sec^{-1}) for states of $1s\,2s\,2p^2$ configuration of Be-like ions.[a]

	Atomic Number															
	$_6C^{+2}$		$_7N^{+3}$		$_8O^{+4}$		$_9F^{+5}$		$_{10}Ne^{+6}$		$_{12}Mg^{+8}$		$_{18}Ar^{+14}$		$_{26}Fe^{+22}$	
State	Auger	x ray	Auger	x ray	Auger	x ray	Auger	x ray	Auger	x ray	Auger	x ray	Auger	x ray	Auger	x ray
$^5P_1$	1.23(−4)	1.61(−6)	2.88(−4)	9.23(−6)	6.17(−4)	4.10(−5)	1.26(−3)	1.51(−4)	2.49(−3)	4.77(−4)	8.69(−3)	3.43(−3)	1.53(−1)	2.58(−1)	1.74	1.91(+1)
$^5P_2$	2.26(−4)	1.68(−6)	4.83(−4)	8.81(−6)	8.99(−4)	3.65(−5)	1.54(−3)	1.27(−4)	2.52(−3)	3.82(−4)	6.15(−3)	2.55(−3)	6.20(−2)	1.57(−1)	5.34(−1)	5.24
$^5P_3$	1.34(−4)	9.56(−7)	4.61(−4)	5.76(−6)	1.31(−3)	2.65(−5)	3.24(−3)	9.97(−5)	7.20(−3)	3.22(−4)	2.76(−2)	2.39(−3)	5.01(−1)	1.95(−1)	6.44	1.02(+1)
$(^3S)^3P_0$	3.84(+1)	8.95(−1)	3.71(+1)	1.95	3.50(+1)	3.74	3.31(+1)	6.53	3.25(+1)	1.06(+1)	3.10(+1)	2.43(1)	3.38(+1)	1.41(+2)	6.72(+1)	6.17(+2)
$(^3S)^3P_1$	3.80(+1)	8.95(−1)	3.66(+1)	1.95	3.44(+1)	3.74	3.28(+1)	6.53	3.21(+1)	1.06(+1)	3.39(+1)	2.37(1)	1.17(+2)	7.69(+1)	6.15(+1)	5.72(+2)
$(^3S)^3P_2$	3.72(+1)	8.95(−1)	3.55(+1)	1.95	3.36(+1)	3.74	3.20(+1)	6.53	3.18(+1)	1.06(+1)	4.83(+1)	2.11(1)	5.26(+1)	1.23(+2)	9.05(+1)	5.22(+2)
$^3D_1$	6.52(+1)	3.15(−1)	8.14(+1)	6.85(−1)	9.44(+1)	1.31	1.05(+2)	2.29	1.14(+2)	3.75	1.26(+2)	9.04	6.49(+1)	1.16(+2)	1.40(+2)	3.27(+2)
$^3D_2$	6.52(+1)	3.15(−1)	8.13(+1)	6.85(−1)	9.44(+1)	1.31	1.05(+2)	2.30	1.14(+2)	3.80	1.08(+2)	1.17(1)	1.26(+2)	7.03(+1)	1.30(+2)	3.58(+2)
$^3D_3$	6.51(+1)	3.15(−1)	8.13(+1)	6.86(−1)	9.42(+1)	1.31	1.05(+2)	2.29	1.15(+2)	3.72	1.29(+2)	8.49	1.53(+2)	4.98(+1)	1.61(+2)	2.27(+2)
$^1D_2$	1.71(+2)	3.10(−1)	1.96(+2)	6.76(−1)	2.13(+2)	1.30	2.26(+2)	2.62	2.40(+2)	3.69	2.55(+2)	8.37	2.68(+2)	4.36(+1)	2.36(+2)	2.17(+2)
$(^1S)^3P_0$	7.54(+1)	4.88(−2)	8.97(+1)	1.03(−1)	1.01(+2)	1.92(−1)	1.10(+2)	3.29(−1)	1.19(+2)	5.32(−1)	1.32(+2)	1.22	1.56(+2)	9.53	1.57(+2)	1.14(+2)
$(^1S)^3P_1$	7.50(+1)	4.88(−2)	8.92(+1)	1.03(−1)	1.01(+2)	1.91(−1)	1.10(+2)	3.27(−1)	1.19(+2)	5.26(−1)	1.31(+2)	1.20	1.49(+2)	1.06(+1)	1.22(+2)	1.53(+2)
$(^1S)^3P_2$	7.42(+1)	4.86(−2)	8.82(+1)	1.02(−1)	9.97(+1)	1.88(−1)	1.09(+2)	3.19(−1)	1.19(+2)	5.07(−1)	1.33(+2)	1.14	1.84(+2)	1.18(+1)	2.33(+2)	7.76(+1)
$^1S_0$	1.27(+2)	3.12(−1)	1.43(+2)	6.81(−1)	1.54(+2)	1.30	1.62(+2)	2.28	1.72(+2)	3.71	1.81(+2)	8.45	2.02(+2)	4.87(+1)	2.23(+2)	2.16(+2)
$^3S_1$	3.29(+1)	3.17(−1)	4.05(+1)	6.90(−1)	4.69(+1)	1.32	5.23(+1)	2.30	5.65(+1)	3.74	6.40(+1)	8.51	8.23(+1)	4.76(+1)	1.28(+2)	1.60(+2)
$^1P_1$	1.21(+1)	9.49(−1)	1.80(+1)	2.06	2.29(+1)	3.95	2.80(+1)	6.88	3.13(+1)	1.21(+1)	3.90(+1)	2.55(+1)	5.28(+1)	1.48(+2)	5.71(+1)	6.66(+2)

[a]Numbers in parentheses stand for powers of ten, e.g., $1.23(-4)=1.23\times10^{-4}$.

TABLE VII. Theoretical Auger x-ray transition rates (in multiple of 10^2 sec^{-1}) for states of $1s\,2p^3$ configuration of Be-like ions.

	Atomic Number																	
	$_6C^{+2}$		$_7N^{+3}$		$_8O^{+4}$		$_9F^{+5}$		$_{10}Ne^{+6}$		$_{12}Mg^{+8}$		$_{18}Ar^{+14}$		$_{26}Fe^{+22}$	
State	Auger	x ray	Auger	x ray	Auger	x ray	Auger	x ray	Auger	x ray	Auger	x ray	Auger	x ray	Auger	xray
$^5S_2$	1.43(−4)	1.48(−3)	4.64(−4)	1.92(−3)	1.27(−3)	2.38(−3)	3.09(−3)	2.90(−3)	6.78(−3)	3.61(−3)	2.59(−2)	6.85(−3)	4.81(−1)	2.25(−1)	7.31	1.29(+1)
$^3S_1$	1.78(−3)	1.25	5.45(−3)	2.73	1.50(−2)	5.22	3.66(−2)	9.12	8.06(−2)	1.48(+1)	3.09(−1)	3.38(+1)	5.35	1.95(+2)	4.94(+1)	7.91(+2)
$^3P_0$	5.57(+1)	2.93(−1)	6.93(+1)	6.40(−1)	7.97(+1)	1.23	8.87(+1)	2.14	9.62(+1)	3.50	1.09(+2)	8.00	1.31(+2)	4.74(+1)	1.41(+2)	2.27(+2)
$^3P_1$	5.57(+1)	2.93(−1)	6.91(+1)	6.40(−1)	8.00(+1)	1.23	8.91(+1)	2.15	9.65(+1)	3.50	1.08(+2)	8.04	1.29(+2)	5.09(+1)	1.41(+2)	3.09(+2)
$^3P_2$	5.57(+1)	2.93(−1)	6.91(+1)	6.40(−1)	7.99(+1)	1.23	8.90(+1)	2.16	9.69(+1)	3.56	1.11(+2)	8.85	1.56(+2)	8.25(+1)	1.71(+2)	3.78(+2)
$^1P_1$	5.37(+1)	9.17(−1)	6.66(+1)	2.00	7.69(+1)	3.83	8.57(+1)	6.69	9.30(+1)	1.09(+1)	1.04(+2)	2.49(+1)	1.25(+2)	1.47(+2)	1.35(+2)	6.77(+2)
$^3D_1$	9.24(+1)	3.12(−1)	1.14(+2)	6.79(−1)	1.31(+2)	1.30	1.45(+2)	2.27	1.57(+2)	3.69	1.76(+2)	8.43	2.05(+2)	5.04(+1)	1.92(+2)	3.27(+2)
$^3D_2$	9.25(+1)	3.12(−1)	1.14(+2)	6.79(−1)	1.31(+2)	1.30	1.45(+2)	2.27	1.57(+2)	3.70	1.75(+2)	8.44	2.05(+2)	4.97(+1)	2.12(+2)	2.40(+2)
$^3D_3$	9.25(+1)	3.12(−1)	1.14(+2)	6.80(−1)	1.31(+2)	1.30	1.46(+2)	2.27	1.58(+2)	3.70	1.76(+2)	8.45	2.09(+2)	4.98(+1)	2.29(+2)	2.37(+2)
$^1D_2$	9.14(+1)	9.37(−1)	1.31(+2)	2.04	1.30(+2)	3.91	1.44(+2)	6.81	1.56(+2)	1.11(+1)	1.71(+2)	2.45(+1)	1.80(+2)	1.14(+2)	2.04(+2)	5.39(+2)

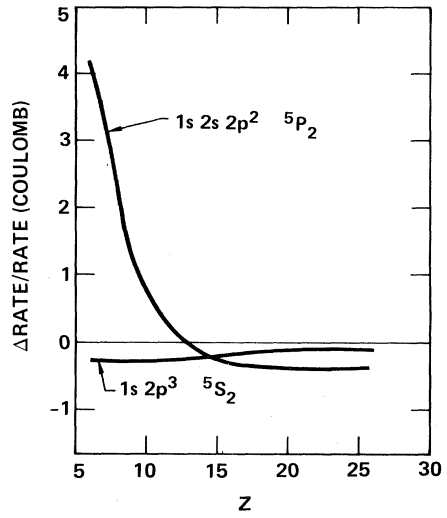

FIG. 1. Relative changes of Auger rates of quintet states due to the inclusion of Breit interaction in the Auger operator as functions of atomic number.

$$\langle f||T_L||i\rangle=\sum_{\alpha=1}^{n_i}\sum_{\beta=1}^{n_f}C_{i\alpha}C_{f\beta}\langle\phi(\Gamma_\beta J')||T_L||\phi(\Gamma_\alpha J)\rangle\ . \tag{11}$$

This CSF matrix element in term can be written as

$$\langle\phi(\Gamma_\beta J')||T_L||\phi(\Gamma_\alpha J)\rangle=\sum_{p,q}d_{pq}^{L}(\beta,\alpha)\langle p||T_L||q\rangle\ . \tag{12}$$

Here, the one-electron matrix elements $\langle P||T_L||q\rangle$ are defined by Grant.[24] The $d_{pq}^{L}(\beta,\alpha)$ are angular factors which depend on the angular momentum and the configurational structure of CSF.[25]

For the electric-dipole transition ($E1$), the one-electron matrix element becomes[24]

$$\langle p||T_1||q\rangle=\left[\frac{\omega}{\pi}\right]^{1/2}(-1)^{j_p-1/2}\times[(2j_p+1)(2j_q+1)]^{1/2}\begin{pmatrix} j_p & 1 & j_q \\ \frac{1}{2} & 0 & -\frac{1}{2}\end{pmatrix}T_1^{(e)}\ , \tag{13}$$

where in Coulomb gauge

$$T_1^{(e)}=\frac{i}{\sqrt{2}}[(k_p-k_q)(I_2^+-2I_0^+)+2I_2^-+2I_0^-] \tag{14}$$

and in length gauge

$$T_1^{(e)}=\frac{3i}{\sqrt{2}}[2J^{(1)}+(k_p-k_q)I_2^++2I_2^-]\ , \tag{15}$$

with

$$\omega=(E_i-E_f)/c\ . \tag{16}$$

The $I_L^{\pm}(\omega)$ and $J^{(L)}(\omega)$ radial integrals are defined as follows:[24,27]

$$I_L^{\pm}(\omega)=\int_0^\infty(P_fQ_i\pm Q_fP_i)j_L(\omega r)dr\ , \tag{17}$$

TABLE VIII. Theoretical Auger and radiative transition rates (in multiple of 10^{12} sec^{-1}) for states of $1s2s^22p$ configuration of Be-like ions.

	$^3P_0$		$^3P_1$		$^3P_2$		$^1P_1$	
ion	Auger	x ray	Auger	x ray	Auger	x ray	Auger	x ray
$_6C^{+2}$	1.03(+2)	2.05(−2)	1.02(2)	1.20(−2)	1.02(2)	2.06(−2)	7.23(1)	6.52(−1)
$_7N^{+3}$	1.18(2)	4.28(−2)	1.18(2)	2.52(−2)	1.17(2)	4.30(−2)	8.15(1)	1.42
$_8O^{+4}$	1.29(2)	7.91(−2)	1.29(2)	4.68(−2)	1.28(2)	7.95(−2)	8.74(1)	2.71
$_9F^{+5}$	1.38(2)	1.34(−1)	1.38(2)	8.01(−2)	1.37(2)	1.35(−1)	9.23(1)	4.72
$_{10}Ne^{+6}$	1.47(2)	2.12(−1)	1.47(2)	1.29(−1)	1.45(2)	2.15(−1)	9.80(1)	7.68
$_{12}Mg^{+8}$	1.58(2)	4.61(−1)	1.59(2)	3.00(−1)	1.56(2)	4.72(−1)	1.05(2)	1.75(1)
$_{18}Ar^{+14}$	1.82(2)	2.30	1.83(2)	2.85	1.83(2)	2.50	1.22(2)	1.01(2)
$_{26}Fe^{+22}$	2.00(2)	7.69	1.92(2)	4.68(1)	1.95(2)	1.01(1)	1.38(2)	4.44(2)

$$J^{(L)}(\omega)=\int_0^\infty (P_fP_i\pm Q_fQ_i)j_L(\omega r)dr\ . \tag{18}$$

III. NUMERICAL METHOD

The energies and wave functions for bound states were calculated using the MCDF model with extended average-level scheme (EAL).[17] In the EAL calculations, the orbital wave functions are obtained by minimizing the statistically averaged energy of all the levels. In our present calculations of Be-like ions, we used 40 CSF functions from $1s^22s^2$, $1s^22s2p$, $1s^22p^2$, $1s2s^22p$, $1s2s2p^2$, and $1s2p^3$. The mixing coefficients C_{ij} [Eq. (6)] were obtained by diagonalizing the energy matrix which includes Coulomb and transverse Breit interactions.[17] The quantum-electrodynamic corrections[23] (QED) were also included in the calculated transition energies.

The Auger energies were obtained by performing separate MCDF calculations for initial and final ionic states (ΔSCF method). However, in the calculations of Auger transition rates, the orbital wave functions from the initial state were used to avoid the complication from nonorthogonality of the initial and final orbital wave functions. The continuum wave functions were generated by solving the Dirac-Fock equations corresponding to final state without the exchange interaction between bound and continuum electrons. The continuum wave functions were then Schmidt orthogonalized to the initial orbital wave functions. The angular factors of the Auger matrix elements $A_{\lambda\lambda'}$, Eq. (8), for the Coulomb and generalized Breit operator, Eq. (2), were obtained by using slightly modified general angular momentum subroutines MCP (Ref. 17) and MCBP (Ref. 23), respectively. The Auger transition rates were then calculated according to Eq. (7).

The radiative $E1$ transition rates were calculated according to Eqs. (10)—(18) for both Coulomb and length gauges. The orbital wave functions and mixing coefficients from MCDF EAL scheme with 40 CSF functions were used in the calculations. This procedure employs the same orthonormal set of orbitals to describe the initial and final states of a radiative transition. The predicted transition energy is used in the evaluation of one-electron dipole matrix element [Eq. (13)]. The angular factors $d^L_{pq}(\beta,\alpha)$ were calculated using general angular momentum code (MCT) for one-electron tensor operator.[17,28]

IV. RESULTS AND DISCUSSION

The calculated K x-ray energies for the $1s2l^n2l'^m$ $(n+m=3)$ configurations of Be-like ions are listed in Tables I and II. The present K x-ray energies for Mg^{+8} agree with the results from $1/Z$ expansion theory[29] within $\sim$1.6 eV. In Table III, the mean transition wavelengths for the $1s2s2p^2\,{}^5P_{1,2,3}-1s2p^3\,{}^5S_2$ transitions from MCDF optimal level (OL),[14] MCDF-EAL with 30 CSF (Ref. 14), and present MCDF-EAL with 40 CSF's are compared with experiments.[11,12,14] The results from the present work are found to agree slightly better with experiments[11,12,14] than previous MCDF calculations.[11,30] However, no improvement for the fine structure of the $1s2s2p^2\,{}^5P_{1,2,3}$ states from present calculations has been attained. The remaining discrepancies between theory and experiment for transition wavelengths are probably due to the inadequacy in the calculations of correlation corrections using the limited configuration interaction approach. The calculated K Auger energies are listed in Tables IV and V. Although the QED corrections to the K x-ray and Auger energies are quite small ($\lesssim$0.3 eV) for $Z\lesssim 12$, these corrections reduce the K transition energies for $_{26}$Fe by $\sim$4 eV.[31]

The total theoretical Auger rates and radiative transition rates from Coulomb gauge for states of $1s2s2p^2$, $1s2p^3$, and $1s2s^22p$ configurations are listed in Tables VI, VII, and VIII, respectively. The K-shell radiative rates from length gauge are larger than the rates from Coulomb gauge by 10—15% at $Z=6$ and by $\sim$3% at $Z=26$. However, for $2s$-$2p$ transitions, they differ by as much as a factor of 2 at $Z=6$. Our present $2s$-$2p$ radiative transition rates from length gauge deviate from the corresponding rates from Refs. 30 and 31 by $\sim$12% at $Z=6$ and by $\sim$4% at $Z=10$. For K x-ray emission rates, the present results from Coulomb gauge agree within $\sim$4% with the values from $1/Z$ expansion theory.[29,32] The present Auger rates, however, differ from the results obtained by using Coulomb wave functions[32] by as much as a factor of 2. In order to study the effect of configuration interaction (CI) on transition energies and transition rates, we also performed single-manifold calculations for $1s2p^3$ configuration for Ne^{+6} ions. The configuration interaction between $1s2s^22p\,{}^{1,3}P$ and $1s2p^3\,{}^{1,3}P$ changes the transition energies for $^{1,3}P$ terms by $\sim$2.4 eV for Ne^{+6} ions. This

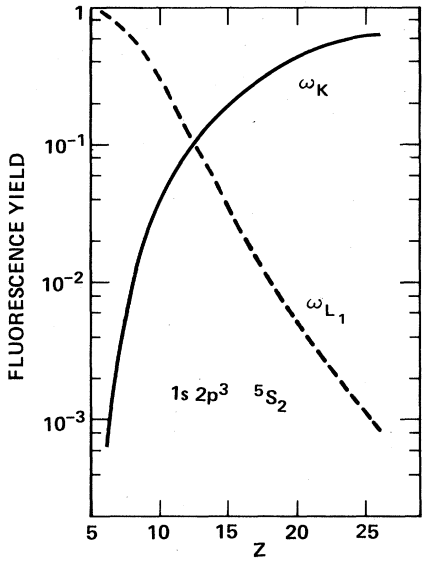

FIG. 2. Fluorescence yields of $1s2p^3\,^5S_2$ state as functions of atomic number. The solid curve indicates the results for K shell, and the broken curve represents the results for L_1 shell.

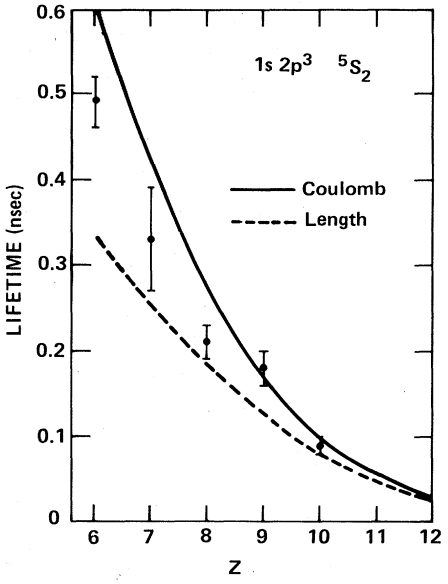

FIG. 3. Lifetime of $1s2p^3\,^5S_2$ state as functions of atomic number. The solid curve represents the results from Coulomb gauge for radiative transitions, and the dashed curve indicates the results from length gauge. The experimental results are from Refs. 11–14.

configuration interaction affects the K x-ray rates for $^{1,3}P$ by only $\sim 5\%$. However, this interaction reduces the Auger rates for $1s2p^3\,^{1,3}P$ terms by $\sim 20\%$. For $^5S_2$ and $^3S_1$ states of $1s2p^3$ configuration, the Auger decay is forbidden in nonrelativistic limit in LS coupling. The CI effect increases the relative position between $^5S_2$, $^3S_1$ and their corresponding ^{1,3}P states. This leads to a large reduction (by $\sim$ a factor of 2–4) in Auger rates for $^5S_2$ and $^3S_1$ states. The Auger rates for states of $1s2p^3$ configuration for Ne^{+6} ion from the present single manifold calculations differ from the nonrelativistic Hartree-Slater results[15] by $\sim 15\%$ because of the difference in orbital wave functions.

The $^3S_1$ state of $1s2p^3$ configuration decays predominantly by K x-ray emission. The Auger decay of this state gains strength from mixing with other triplet and singlet states through intermediate coupling. The Auger rate of this state increases over four orders of magnitude from $Z=6$ to 26.

For ^5S state of $1s2p^3$ and ^5P states of $1s2s2p^2$ configurations, both Auger and dipole K x-ray transitions are forbidden in the nonrelativistic approximation. The quintet states can decay radiatively only by higher multipole K x-ray emission, or by $E1$ transitions made possible by mixing with singlet and triplet states through intermediate coupling. The ^5S state can also decay via $1s2p^3\,^5S_2 \rightarrow 1s2s2p^2\,^5P_{1,2,3}E1$ transitions. Auger decay of the quintet states can occur through mixing with singlet and triplet states or by magnetic interaction. The importance of the Breit interaction in the decay of high spin states has been noted for Li-like ions.[9,10] In the present work, a similar situation has been found for quintet states. The magnetic interaction increases the Auger rates for $1s2s2p^2\,^5P$ states by as much as a factor of 5 for $Z=6$ and reduces the Auger rates by $\sim 40\%$ at $Z=26$ (Fig. 1). The magnetic interaction also reduces the Auger rates for $1s2p^3\,^5S_2$ states by $\sim 25\%$ for $Z \lesssim 15$ (Fig. 1). As Z increases, the contributions due to the mixing with singlet and triplet states through spin-orbit interaction become predominant.[9]

The K fluorescence yields (ω_k) and L_1 fluorescence yields (ω_{L_1}) for the $1s2p^3\,^5S_2$ states are shown in Fig. 2. The decay of the $^5S_2$ state is dominated by the $2s$-$2p$ $E1$ transition for $Z \lesssim 8$. For $9 \lesssim Z \lesssim 25$, Auger transition is the dominant branch and for $Z > 25$, the K x-ray emission becomes the most important decay mode (Fig. 2).

The lifetime of the $1s2p^3\,^5S_2$ state from present calculations including radiative and radiationless transitions is compared with experiments[11–14] in Fig. 3. The theoretical results using radiative rates from length gauge underestimate the lifetime while the results from Coulomb gauge slightly overestimate the lifetime. Previous MCDF calculations[12,14] for the lifetime of the $1s2p^3\,^5S$ state ignore the contributions from radiationless transitions. However, our present work indicates that the Auger transition plays a key role in the decay of this high-spin state. As for the ^4P states of $1s2l2l'$ configurations of Li-like ions,[9], the effects of relativity are very important in the decay of ^5S and ^5P states of $1s2l^n2l'^m$ $(n+m=3)$ configurations of Be-like ions. Their inclusion in the theoretical description is essential for the correct prediction of the lifetimes and fluorescence yields of these high-spin states.

ACKNOWLEDGMENT

This work was performed under the auspices of the U.S. Department of Energy by the Lawrence Livermore National Laboratory under Contract No. W-7405-ENG-48.

[1]V. A. Boiko, A. Ya Faenov, and S. A. Pikuz, J. Quant. Spectrosc. Radiat. Transfer **19**, 11 (1978).
[2]E. Ya Gol'ts, U. I. Zitnik, E. Ya Kononov, S. L. Mandel'shtam, and Yu V. Sidel'nikov, Dokl. Akad. Nauk SSSR **220**, 560 (1975) [Sov. Phys.—Dokl **20**, 49 (1975)].
[3]E. V. Aglitsky, V. A. Boiko, S. M. Zaharov, S. A. Pikuz, and A. Yu Faenov, Kvant. Elektron. (Moscow) **1**, 908 (1974) [Sov. J. Quantum Electron. **4**, 500 (1974)].
[4]C. P. Bhalla, A. H. Gabriel, and L. P. Presnyakov, Mon. Not. R. Astron. Soc. **172**, 359 (1975).
[5]K. T. Cheng, C. P. Lin, and W. R. Johnson, Phys. Lett. **48A**, 437 (1974).
[6]L. A. Vainshtein and U. I. Safronova, At. Data Nucl. Data Tables **21**, 50 (1978).
[7]A. H. Gabriel, Mon. Not. R. Astron. Soc. **160**, 99 (1972).
[8]M. H. Chen and B. Crasemann, Phys. Rev. A **12**, 959 (1975).
[9]M. H. Chen, B. Crasemann, and H. Mark, Phys. Rev. A **24**, 1852 (1981); **27**, 544 (1983); **26**, 1441 (1982).
[10]C. P. Bhalla and T. W. Tunnell, Z. Phys. A **303**, 199 (1981); in *Inner-Shell and X-ray Physics of Atoms and Solids,* edited by D. J. Fabian, H. Kleipoppen, and L. M. Watson (Plenum, New York, 1981), p. 285.
[11]I. Martinson, B. Denne, J. O. Ekberg, L. Engström, S. Huldt, C. Jupèn, U. Litzén, S. Mannervik, and A. Trigueiros, Phys. Scr. **27**, 201 (1983).
[12]H. G. Berry, R. L. Brooks, K. T. Cheng, J. E. Hardis, and W. Ray, Phys. Scr. **25**, 391 (1982).
[13]A. E. Livingston and S. J. Hinterlong, Phys. Lett. **80A**, 372 (1980).
[14]A. E. Livingston (private communicaton).
[15]C. P. Bhalla, J. Electron Spectrosc. Relat. Phenom. **7**, 287 (1975); J. Phys. B **8**, 2792 (1975).
[16]M. H. Chen and B. Crasemann, Phys. Rev. A **10**, 2232 (1974).
[17]I. P. Grant, B. J. McKenzie, P. H. Norrington, D. F. Mayers, and N. C. Pyper, Comput. Phys. Comm. **21**, 207 (1980).
[18]W. Bambynek, B. Crasemann, R. W. Fink, H. U. Freund, H. Mark, C. D. Swift, R. E. Price, and P. V. Rao, Rev. Mod. Phys. **44**, 716 (1972).
[19]M. H. Chen, E. Laiman, B. Crasemann, and Hans Mark, Phys. Rev. **19**, 2253 (1979).
[20]H. A. Bethe and E. E. Salpeter, *Quantum Mechanics of One- and Two-Electron Systems* (Springer, Berlin, 1957).
[21]J. B. Mann and W. R. Johnson, Phys. Rev. A **4**, 41 (1971).
[22]U. Fano, Phys. Rev. **140**, A67 (1965).
[23]B. J. McKenzie, I. P. Grant, and P. H. Norrington, Comput. Phys. Comm. **21**, 233 (1980).
[24]I. P. Grant, J. Phys. B **7**, 1458 (1974).
[25]J. Hata and I. P. Grant, J. Phys. B **14**, 2111 (1981).
[26]M. H. Chen, B. Crasemann and H. Mark, Phys. Rev. A **24**, 1852 (1981).
[27]H. R. Rosner and C. P. Bhalla, Z. Phys. **231**, 347 (1970).
[28]N. C. Pyper, I. P. Grant, and N. Beatham, Comput. Phys. Comm. **15**, 387 (1978).
[29]U. I. Safronova and V. S. Senashenko, Phys. Scr. **25**, 37 (1982).
[30]J. Hata and I. P. Grant, J. Phys. B **16**, L125 (1983).
[31]K. N. Huang, M. Aoyagi, M. H. Chen, B. Crasemann, and H. Mark, At. Data Nucl. Data Tables **18**, 243 (1976).
[32]V. I. Safronova and T. G. Lisina, At. Data Nucl. Data Tables **24**, 49 (1979).